Parametric Analysis of a High Temperature Packed Bed Thermal Storage Design for a Solar Gas Turbine

P. Klein[a,b,*], T.H. Roos[b], T.J. Sheer[a]

[a] *School of Mechanical, Industrial and Aeronautical Engineering, University of the Witwatersrand, Johannesburg, South Africa*
[b] *Council for Scientific and Industrial Research, Pretoria, South Africa*

Abstract

The development of a high temperature Thermal Energy Storage (TES) system will allow for high solar shares in Solar Gas Turbine (SGT) plants. In this research a pressurised storage solution is proposed that utilises a packed bed of alumina spheres as the storage medium and air from the gas turbine cycle as the heat transfer fluid. A detailed model of the storage system is developed that accounts for transient heat transfer between discrete fluid and solid phases. The model includes all relevant convective, conductive and radiative heat transfer mechanisms and is validated against high temperature experimental data from a laboratory scale test facility. The validated model is further utilised to conduct a parametric design study of a nominal six hour TES (1.55 MWh_{th}) for a micro-gas turbine. The concepts of utilisation factor and storage efficiency are introduced to determine the optimal storage design. The results of the study indicate that a storage efficiency of 88% and utilisation factor of 85% can be achieved when combining thermal storage and hybridisation with fossil fuels.

Keywords: Concentrating solar power, Thermal storage, Packed bed, Sensible heat, Gas turbine

*Corresponding Author: Peter Klein, pklein@csir.co.za, +27-12-841-3631

1. Introduction

A concentrated solar-hybrid gas turbine cycle offers new opportunities for off-the-grid and grid supportive power generation. This technology has the potential to provide fully dispatchable power, while remaining cost competitive with diesel generators. Recuperated gas micro-turbines are applicable to off-the-grid applications as they can be manufactured in the 100-350 kW_e range, with cycle efficiencies of up to 30%. They also require no cooling water and are readily hybridisable with fossil fuels. As stated by Klein et al. (2014a), the overall plant efficiency can be further increased by employing an absorption chiller or multi effect desalination unit, powered by thermal energy exhausted from the gas turbine.

During periods when insolation is not available, hybridised Solar Gas Turbines (SGT) can produce power by operating on backup fossil fuel. However, in order to produce dispatchable power at high solar shares, a high temperature Thermal Energy Storage (TES) system is proposed. As demonstrated by Amsbeck et al. (2010) the inclusion of a nine hour TES could increase the solar share of a gas micro-turbine from 25% to 82%.

Ceramic heat regenerators are suited to high temperature TES applications where the heat transfer fluid is air. Packed bed regenerators exhibit high heat transfer rates, offering the potential for efficient, low cost storage (Zunft et al., 2014). This technology was successfully integrated into a Concentrating Solar Power (CSP) plant during the TSA-PHOEBUS (Technology program Solar Air Receiver) project. Too et al. (2012) conducted a review of suitable TES for gas turbines and found a packed bed to be an efficient solution in the near term. Amsbeck et al. (2010) also proposed the use of a pressurised packed bed TES for a gas micro-turbine.

This research is focussed on the design analysis of a pressurised packed bed regenerative thermal storage system for a gas micro-turbine. A comprehensive storage model is developed and validated against experimental data. The validated model is used to conduct a parametric design study to determine the

optimal storage configuration for a 1.55 MWh_{th} (nominal six hours for the chosen turbine) thermal storage system.

2. Hybridised solar gas turbine cycle

The proposed SGT cycle is based on the Turbec T100 gas turbine. This commercially available micro-turbine is designed for the co-generation of electricity and hot water (Turbec, 2006). The T100 was utilised in the EUFP7 SOLHYCO project (SOlar HYbrid CO-generation) that developed a SGT system based on a high temperature tubular receiver (Amsbeck et al., 2010). AORA solar currently operates two solar gas turbine plants based on the T100 (Aora, n.d). The turbine produces 100 kW_e of electricity and 170 kW_{th} of thermal energy at standard ISO conditions, with a turbine inlet temperature of 950 ℃ and pressure ratio of 4.5. A schematic of the cycle, including pressurised thermal storage, is presented in Fig. 1.

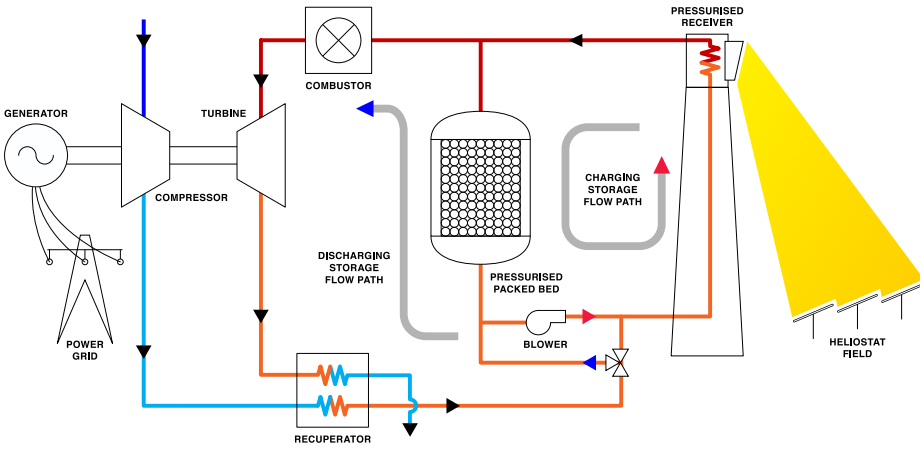

Figure 1: Schematic of micro-gas turbine cycle with thermal storage

The cycle consists of a recuperated gas micro-turbine that is converted to accept thermal energy from a pressurised air receiver. Hybridisation is achieved by placing the combustion chamber from the gas turbine in series with the solar receiver, thus allowing boosting of the turbine inlet temperature. The thermal

storage is connected in a parallel configuration with the receiver. Excess thermal energy is transferred to the storage using a blower that re-circulates air through the receiver and packed bed. Energy is withdrawn from the storage by diverting the turbine airflow through the packed bed (Klein et al., 2014b).

3. Literature review on high temperature packed bed thermal storage

Forced convection heat transfer in randomly packed beds has received significant research attention over the past decades. Early studies were based on the analytical solutions to the Schumann model (Schumann, 1929; Klinkenberg, 1948). Due to the limited applicability of the analytical solutions, further investigations relied on numerical modelling (Beasley and Clark, 1984; Ismail and Stuginsky, 1999). Wakao and Kaguei (1982) provide an overview of convective heat transfer models and constitutive correlations for randomly packed beds. Previous research papers are predominately focussed on low temperature systems with a maximum temperature below 200 ℃. Fewer studies are available on heat transfer in packed beds where the charging temperature exceeds 600 ℃.

3.1. Gas heat transfer fluid

Jalalzadeh-Azar et al. (1996) developed a high temperature test facility to study the heat transfer in a packed bed of zirconia pellets for industrial heat recovery. The heat transfer fluid in the system was flue gas from a 350 kW_{th} burner for the charging cycle and air for the discharging cycle. The effects of gas radiation and intra-particle conduction were studied. The convective heat transfer correlations of Bradshaw et al. (1970) and Wakao and Kaguei (1982) were found to be suitable up to a temperature of 960 ℃. Adebiyi et al. (1998) also presented a numerical model of this zirconia TES system which was validated against experimental data up to a temperature of 800 ℃. The model was further used to conduct a parametric analysis of the system based on first and second law efficiency metrics.

A packed bed of composite salt/ceramic particles was developed by the German Aerospace Institute (DLR), Didier Ceramics and Stuttgart University for

high temperature thermal storage systems (Tamme et al., 1990). The micro-encapsulation of a phase change material within the pores of a ceramic structure was aimed at improving the energy density of the storage material. Composite SiO_2/Na_2SO_4 pellets were successfully developed and tested with respect to thermal performance and physical stability. However, testing conducted by Jalalzadeh-Azar et al. (1997) indicated that a SiO_2/Na_2SO_4 material was inferior to zirconia in high temperature packed bed TES experiments. The testing involved charging and discharging cycles, using flue gas and air as the respective heat transfer fluids.

Glück et al. (1991) developed a packed bed test facility to test heat storage materials up to a maximum temperature of 1300 ℃. The storage system was charged using flue gas from a burner at atmospheric pressure and discharged using air at a pressure of 21 bar, thus demonstrating the operation of a pressurised packed bed storage system.

The heat transfer in a high temperature packed bed was analysed by Du Toit et al. (2006) for nuclear applications. Detailed heat transfer and fluid flow models were presented for the system and solved using the systems based network CFD code FLOWNEX. The model was validated against experimental data from the SANA experiments, conducted by Niessen and Stöcker (1997). Both nitrogen and helium were tested as heat transfer fluids for the case of natural convection heat transfer in the packed bed.

A high temperature rock bed thermal storage system was studied by Zanganeh et al. (2012) using air as the heat transfer fluid at temperatures ranging between 20 ℃ and 650 ℃. A numerical model of the system was formulated and validated against experimental data from a pilot scale test facility. The modelling accounted for temperature dependent changes in the thermophysical properties. A design study was conducted for an array of two 7.2 GWh_{th} packed bed storage units.

A parametric analysis of a high temperature TES system for solar thermal applications was presented by Mongibello et al. (2013). The system utilised CO_2 as the heat transfer fluid and packed beds of both alumina and zirconia

particles were analysed over the temperature range 670-850 ℃. The numerical heat transfer model was validated against experimental data over the range 100-350 ℃.

Avila-Marin et al. (2014) described a high temperature regenerative thermal storage system for CSP plants based on air cooled receivers. This research was aimed at characterising four types of commercially available alumina spheres in a laboratory scale test facility. A numerical model of the system was developed and compared to experimental data up to a maximum temperature of 640 ℃.

3.2. Liquid heat transfer fluid

Thermocline energy storage in packed beds has also been studied using molten salt as the heat transfer fluid. Typical molten salts used in CSP applications, such as nitrate Solar Salt or HITEC salt, are limited to a maximum temperature below 600 ℃ (Bradshaw and Siegel, 2008). Therefore they cannot be used with the gas turbine cycle. However, the modelling and parametric studies on the packed bed heat transfer are related to the current work. Thus a brief literature review of this research is included for completeness.

Pacheco and Showalter (2002) analysed a packed bed, molten salt TES using the one-dimensional Schumann equations. The results of this study predicted a theoretical storage capacity of 69%. Modi and Pérez-Segarra (2014) also employed a one-dimensional heat transfer model that included thermal losses from the bed and temperature dependent thermophysical properties of the molten salt. Cyclic behaviour of the system was analysed for three different liquid heat transfer fluids.

Yang and Garimella (2010a) developed a detailed axisymmetric model of the heat transfer and fluid flow in a packed bed molten salt TES system. This model was used to investigate the effects of tank height, salt flow rate and particle size on the discharging behaviour of an adiabatic system. Yang and Garimella (2010b) extended this model to include a non adiabatic boundary condition at the tank wall.

Xu et al. (2012a) investigated the effects of different empirical correlations for the interstitial heat transfer coefficient and effective thermal conductivity in a packed bed. This modelling indicated that the use of different empirical constitutive correlations had a negligible effect on the predicted thermal performance. Decreasing the convective heat transfer coefficient or increasing the thermal conductivity of the particles was shown to decrease the discharging time and TES efficiency. This model was used by Xu et al. (2012b) to analyse the effects of porosity, flow rate, inlet temperature and thermal losses on the thermal performance of the packed bed molten salt TES system.

4. Mathematical modelling of TES system

4.1. Governing equations

The simulated storage system consists of a cylindrical packed bed with an insulated wall. The governing equations are formulated in a two-dimensional, axisymmetric coordinate system, using a volume averaged approach. The dynamic two-phase model accounts for discrete fluid and solid phases which exchange energy via convection. The individual solid particles are modelled as a single continuous phase, assuming no intra-particle temperature gradients. The thermophysical properties of the fluid and solid phases are assumed temperature invariant. As described by Zanganeh et al. (2012), the dominant temperature dependent property is the solid phase heat capacity. The temperature dependent heat capacity of candidate ceramic storage materials is presented by Klein et al. (2014b). The materials considered in the current study undergo small changes in heat capacity when the temperature range of analysis is above 350 ℃. Thus the assumption of constant thermophysical properties improves the simulation time and does not introduce solution errors. This was confirmed by comparing the constant property model to a variable property model.

The energy equations for the fluid and solid phases are given by:

$$\epsilon\rho_f c_f \frac{\partial T_f}{\partial t} + \rho_f c_f U_z \frac{\partial T_f}{\partial z} = h_{\mathrm{fs}} a_p \left(T_s - T_f\right) + \nabla \cdot \left(k_{\mathrm{eff,f}} \nabla T_f\right) \tag{1}$$

and

$$(1-\epsilon)\rho_s c_s \frac{\partial T_s}{\partial t} = h_{\text{fs}} a_p \left(T_f - T_s\right) + \nabla \cdot \left(k_{\text{eff,s}} \nabla T_s\right) \tag{2}$$

The energy equation for the packed bed wall is:

$$\rho_w c_w \frac{\partial T_w}{\partial t} = \nabla \cdot \left(k_w \nabla T_w\right) \tag{3}$$

4.2. Constitutive equations

Due to the confining effect of the wall on randomly packed particles, non-uniform radial variations in void fraction occur in packed beds. This effect is included in the current model through the correlation of Hunt and Tien (1990) where:

$$\epsilon(r) = \epsilon_\infty \left(1 + \left(\frac{1-\epsilon_\infty}{\epsilon_\infty}\right) \exp\left(-6\frac{R-r}{d_p}\right)\right) \tag{4}$$

The higher void fraction at the bed wall introduces a velocity channelling effect, whereby the fluid velocity is higher in the near wall region than in the centre of the bed. Assuming axisymmetric and fully developed flow, the profile is resolved by solving the extended Brinkman equation as proposed by Vortmeyer and Schuster (1983), where:

$$\frac{\Delta P}{L_z} = -f_1(r) U_z(r) - f_2(r) \left(U_z(r)\right)^2 + \frac{\mu_{\text{eff}}}{r} \frac{\partial}{\partial r}\left(r \frac{\partial U_z(r)}{\partial r}\right) \tag{5}$$

where

$$f_1(r) = C_A \frac{(1-\epsilon(r))^2}{\epsilon(r)^3} \frac{\mu_f}{d_p^2} \tag{6}$$

and

$$f_2(r) = C_B \frac{(1-\epsilon(r))}{\epsilon(r)^3} \frac{\rho_f}{d_p} \tag{7}$$

subject the the boundary conditions:

$$\frac{\partial U_z(0)}{\partial r} = 0 \tag{8}$$

$$U_z(R) = 0 \tag{9}$$

The coefficients C_A and C_B are given the values of 150 and 1.75 respectively. Authors such as Macdonald et al. (1979) have proposed different values for these coefficients. However, these only influence pressure drop but not the shape of

the channelling profile. The effective viscosity is calculated using the correlation proposed by Giese et al. (1998).

The inter-phase heat transfer coefficient is calculated using the correlation of Gunn (1978), which is valid over the void fraction range $0.35 \leq \epsilon \leq 1$ and up to a Reynolds number of 10^5:

$$\begin{aligned} \mathrm{Nu}_p = \left(7 - 10\epsilon + 5\epsilon^2\right)\left(1 + 0.7\mathrm{Pr}^{0.33}\mathrm{Re}_p^{0.2}\right) \\ + \left(1.33 - 2.4\epsilon + 1.2\epsilon^2\right)\mathrm{Pr}^{0.33}\mathrm{Re}_p^{0.7} \end{aligned} \tag{10}$$

Following from Jeffreson (1972), the isothermal particle assumption can be relaxed by modifying the inter-phase heat transfer coefficient according to

$$h_{\mathrm{fs}} = \frac{h_p}{1 + 0.2\mathrm{Bi}_p} \tag{11}$$

The heat transfer surface area per unit volume of the particles is:

$$a_p = \frac{6\left(1 - \epsilon\right)}{d_p} \tag{12}$$

The inter-particle heat transfer by conduction and radiation is calculated using the Zehner-Bauer-Schlünder (IAEA, 2001) model that accounts for three modes of heat transfer:

$$k_{\mathrm{eff,s}} = k_{\mathrm{eff}}^{sr} + k_{\mathrm{eff}}^{sf} + k_{\mathrm{eff}}^{sc} \tag{13}$$

where k_{eff}^{sr} represents the combined heat transfer by radiation between particles and by conduction through the particles; k_{eff}^{sf} represents heat transfer by conduction through the particles and the stagnant fluid; and k_{eff}^{sc} represents the heat transfer by conduction through the particles and the contact points between particles k_{eff}^{sc} (Visser et al., 2008).

The effective fluid conductivity term represents the heat transport through axial and radial dispersion (braiding effect) and is given by:

$$k_{\mathrm{eff,f}} = C_d \mathrm{Re}_p \mathrm{Pr} \tag{14}$$

Experimental data indicates that the thermal dispersion effect is anisotropic. As described by Beasley and Clark (1984), the value of C_d is 0.1 in the radial direction and between 0.2 and 1 in the axial direction. Jalalzadeh-Azar et al.

(1996) neglected axial dispersion in the modelling of a high temperature packed bed. Wakao and Kaguei (1982) recommend a value of 0.5 in the axial direction and 0.1 in the radial direction. Values of 0.3 and 0.1 were chosen for the axial and radial dispersion coefficients respectively, as these best represented the experimental data. Both $k_{\text{eff,f}}$ and $k_{\text{eff,s}}$ were modified within the near wall region to account for the local porosity increase.

4.3. Boundary and initial conditions

The computational domain is divided into two regions, namely the packed bed and container wall. The boundary conditions for the simulations are presented in Fig. 2. The modelled wall consists of an inner insulation layer and an outer steel pressure vessel with an assumed thickness of 10 mm. The insulation layer is made from micro-porous insulation material. The model includes the exchange of energy between the solid pebbles and the wall, based on the work of Visser et al. (2008). In order to suppress natural convection effects the air flow enters from the top of the packed bed during charging and from the base during discharging. The charging temperature (red) is 950 ℃ while the discharging inlet temperature is 600 ℃ (blue).

4.4. Numerical discretisation

The governing energy equations are solved using the numerical technique of Orthogonal Collocation on Finite Elements (OCFE), with implicit time stepping. Temporal discretisation is achieved using the second order backward difference scheme:

$$\frac{\partial T}{\partial t} = \frac{3T^n - 4T^{n-1} + T^{n-2}}{2\Delta t} \tag{15}$$

OCFE is advocated for resolving partial differential equations involving steep gradients in localised sections of the problem domain (Finlayson, 1980). This method combines the high accuracy of orthogonal collocation with the flexibility of the finite element method. The cubic Hermite polynomials are chosen as the basis function for the collocation procedure. These functions have continuous point values and first derivatives at the element boundaries, making them an

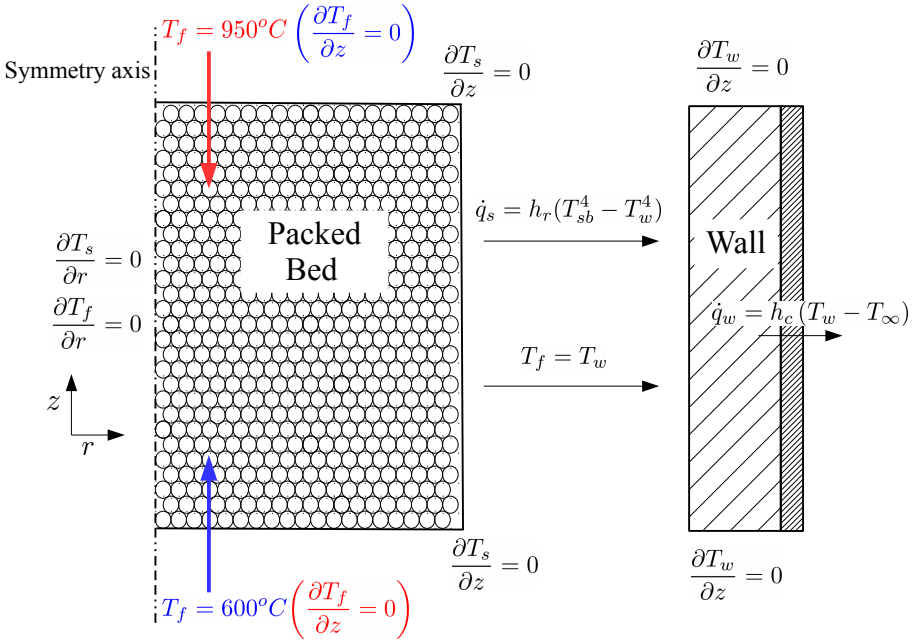

Figure 2: Boundary conditions for packed bed and wall regions

efficient basis function for OCFE. For example, the fluid temperature in the ab_{th} element, where r is located between r_a and r_{a+1} and z between z_b and z_{b+1}, is approximated by:

$$T_f^{ab}(r,z,t) = \sum_{i=1}^{4}\sum_{j=1}^{4} \phi_{ij}^{ab}(t) H_i(u) H_j(v) \tag{16}$$

where

$$u = \frac{r - r_a}{r_{a+1} - r_a} = \frac{r - r_a}{\Delta r_a} \tag{17}$$

and

$$v = \frac{z - z_b}{z_{b+1} - z_b} = \frac{z - z_b}{\Delta z_b} \tag{18}$$

The Hermite polynomials are defined on the unit square as:

$$H_1(u) = (1+2u)(1-u)^2 \tag{19}$$

$$H_2(u, \Delta r_a) = u(1-u)^2 \Delta r_a \tag{20}$$

$$H_3(u) = (3-2u)u^2 \tag{21}$$

$$H_4(u, \Delta r_a) = (u-1)u^2 \Delta r_a \tag{22}$$

4.5. Comparison of developed model with existing models

The present model is comprehensive and addresses all relevant heat transfer mechanisms in the high temperature packed bed. Two key areas exist where there is an improvement over existing packed bed heat transfer models: 1) the inclusion of the local porosity increase at the bed wall and the associated wall channelling flow effect; 2) the in-depth treatment of radiation in the packed bed, via the modified ZBS effective conductivity correlation and the radiation boundary condition between solid particles and the bed wall.

5. TES model validation

A high temperature packed bed test facility was developed to validate the TES model. The facility utilises a 45 kW_{th} LP gas burner to heat a packed bed of alumino-silicate particles. A diagram of the test facility is shown in Fig. 3. Details of the testing programme are provided in Klein et al. (2014b). Tests were conducted over the temperature ranges 350-900 ℃ and 600-900 ℃. A blower failure during the 600-900 ℃ heating test resulted in a limited charging data set. Thus for the purposes of this paper the model was validated using the experimental data over the 350-900 ℃ range. Although this temperature range is large, the normalised changes in solid heat capacity are small and therefore the constant property assumption remains valid. A full cooling test was achieved over the 600-900 ℃ temperature range, and the trends in experimental and numerical data are consistent with those presented in Fig. 4.

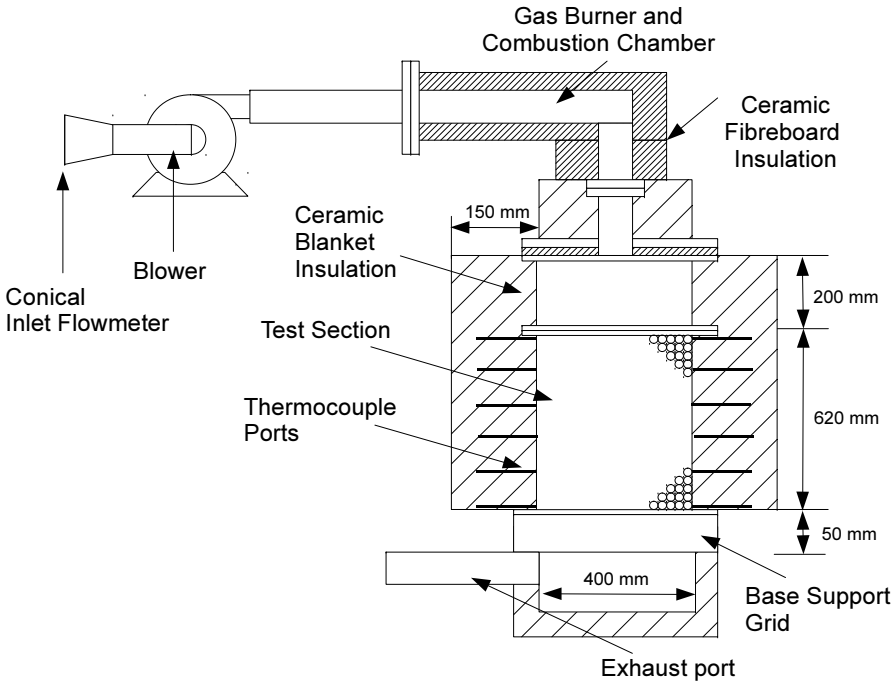

Figure 3: Diagram of the high temperature packed bed test facility (Klein et al., 2014b)

5.1. Axial temperature profiles

Figure 4 shows the predicted and measured axial temperature profiles along the packed bed centreline for the heating and cooling tests. There is good agreement between the TES model and the experimental data. The shape and position of the thermocline in the test facility is well captured by the model. The model underestimates the rate of heating/cooling at the measurement position $z/L_z = 0.18$. This is caused by a lack of a diffuser at the packed bed inlet, which introduces a jet effect onto the top layers of particles. As the flow penetrates deeper into the bed this effect dissipates. For the measurement positions where $z/L_z \geq 0.34$ there is good agreement between the model and experimental data for both heating and cooling cycles. Therefore the model can be used with confidence to predict the axial temperature front in a high temperature packed bed TES.

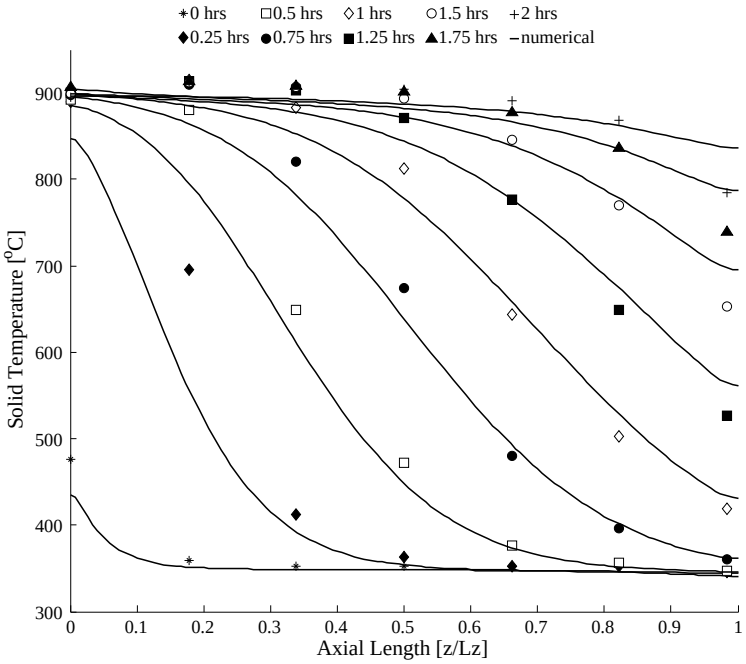

(a) Heating test over 350-900℃ temperature range, $\dot{m}_f$=83.9 kg/h

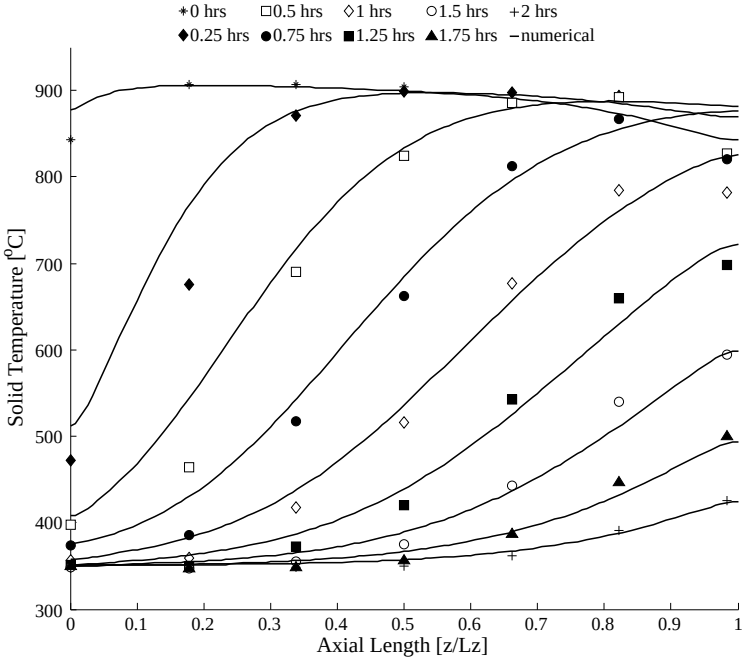

(b) Cooling test over 350-900℃ temperature range $\dot{m}_f$=90.8 kg/h

Figure 4: Comparison between predicted and measured axial solid temperature profiles

5.2. Radial temperature profiles

Temperature measurements were taken at the centre of a pebble adjacent to the bed wall ($r = 0.19$ m) on three axial levels in the packed bed. These measurements are compared to the solid temperature at the bed centreline for each level in Fig. 5. Despite the complex heat transfer at the bed wall, the predicted temperature profiles match the measurements with good accuracy. During the initial stages of heating, the temperature of the solid close to the wall increases faster than in the core region of the packed bed. This is due to the preferential flow in the near wall region. As the temperature of the bed increases, the rate of lateral heat losses through the wall also increases. This causes a shift in the temperature profiles over time to one dominated by heat losses at the wall. In the cooling cycle, the wall channelling and heat losses preferentially cool the near wall region, causing a larger difference between the centreline and wall region solid temperatures.

5.3. Measurement uncertainties

The uncertainty calculated for the conical inlet discharge coefficient was 1.9%, leading to an uncertainty on the mass flow rate of 3.9%. The temperature measurement error on the Type-K thermocouples was taken as the standard reference of 0.75% of the measured temperature value. The uncertainty associated with the placement of the fluid and solid thermocouples was half a particle diameter (≈10 mm) in the axial direction. At the bed centreline the placement uncertainty of the thermocouples was ±5 mm in the radial direction and at the bed wall ±2 mm in the radial direction.

6. Material selection

Due to the high temperature nature of the TES system only ceramic filler materials are considered in this analysis. Suitable storage materials have the following characteristics: 1) high volumetric heat capacity; 2) high operating temperature capability (1000 ℃); 3) good thermal conductivity; 4) resistance to thermal shock; 5) low cost.

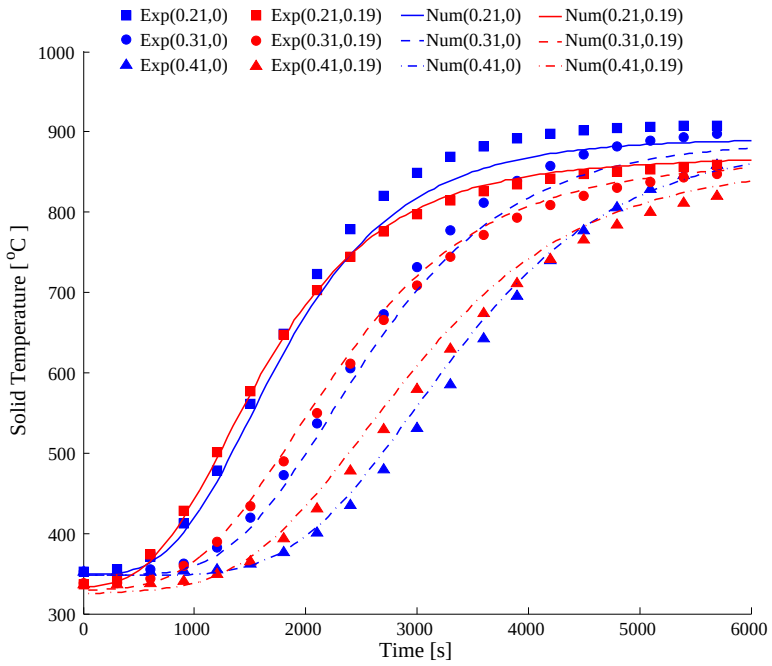

(a) Heating test over 350-900℃ temperature range, $\dot{m}_f$=83.9 kg/h

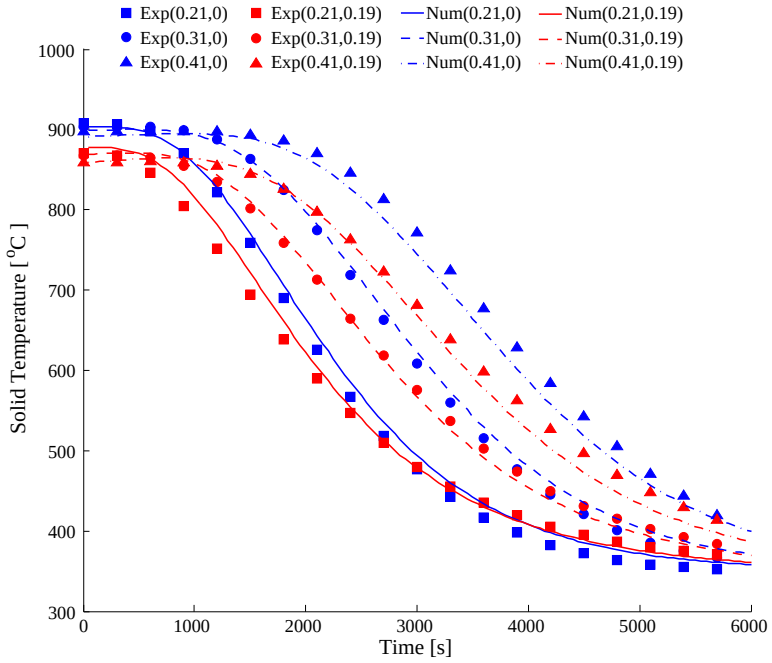

(b) Cooling test over 350-900℃ temperature range, $\dot{m}_f$=90.8 kg/h

Figure 5: Comparison between predicted and measured radial solid temperature profiles

Alumina and zirconia are recommended in the literature as suitable high temperature TES materials (Mongibello et al., 2013; Avila-Marin et al., 2014). The thermophysical properties of these candidate materials are presented in Table 1. Alumina spheres can be sourced in different grades of purity. High-alumina spheres typically have an alumina content greater than 92%, while lower purity alumina spheres are an alumino-silicate material which is predominately SiO_2. Due to the pressurised nature of the storage there is a strong economic driver to reduce the volume of the storage. The density of the high alumina spheres is between 3.6 kg/m^3 and 3.9 kg/m^3, depending on the purity and sintering process. Zirconia was advocated by Jalalzadeh-Azar et al. (1996) and Adebiyi et al. (1998) as an efficient high temperature thermal storage medium. Yttria stabilised zirconia has a density of between 5.4 kg/m^3 and 6 kg/m^3.

In order to estimate the costs of each material a series of quotes were obtained from ceramic manufacturers. The costs provided in Table 1 represent an average of the quotes obtained (excluding shipping costs). Bindra et al. (2013) estimate the cost of alumina spheres for TES at \$100/ft^3 ($\epsilon = 0.35, \rho_s = 3.9$ g/cm^3). This equates to a cost of ≈ 1.4 \$/kg, which is in-line with the estimation made in this work. Zirconia as a heat storage material is more expensive than alumina for two reasons: 1) the higher cost of the raw material and 2) the lower specific heat capacity. In order to store the same amount of energy the storage mass of a zirconia bed would be double that of alumina, while the alumina bed maintains a better volumetric energy storage density. Thus even if the cost of the zirconia material per kilogram was comparable with the alumina, the overall material cost would be double that of the alumina bed. Thus alumina was chosen as the storage material for further analysis due to its cost effectiveness.

Table 1: Heat storage properties of candidate ceramic core materials

Material	ρ_s [kg/m^3]	c_s [J/kgK]	k_s [W/mK]	Q_{vol} [kWh$_{\text{th}}$/m^3][1]	Cost [\$/kg]	Cost [\$/kWh$_{\text{th}}$][1]
Alumina	3.6	1.23	5.4	258	1.3	10.9
Zirconia	5.4	0.62	2.5	195	25.2	418

[1] Calculated assuming $\epsilon = 0.4$, $\Delta T = 350$ K

7. Parametric design study

The validated TES model was used to conduct a parametric design study for a six hour TES for the Turbec T100 turbine. The plant location was Pretoria, South Africa, with an elevation of 1366 m above sea level. The study involved fixing the volume of the packed bed at 7 m^3, while varying the bed aspect ratio ($\alpha = L_z/D$) and particle diameter. The volume was calculated assuming a nominal six hour storage system. The aspect ratios that are considered in this work are: $\alpha = 1, 2, 3, 4, 5$. For each aspect ratio four particle diameters are simulated: $d_p = 10, 16, 25, 50$ mm.

7.1. Solar multiple and plant data

The Solar Multiple (SM) is defined as the thermal power generated by a given solar field at design point, relative to the thermal power required to operate the turbine at the design point. A SM greater than one is required when implementing thermal storage. The plant design used in this research is based on work conducted by the Council for Scientific and Industrial Research and the German Aerospace Center (DLR) as part of the Integrated Resource Infrastructure Platform (IRIP) (Roos et al., 2015). The power block parameters for the Turbec T100PH gas turbine are:

- Compressor inlet air temperature and pressure: 25 ℃ and 88 kPa
- Turbine power at operating conditions: 73 kW$_{\text{e}}$
- Turbine efficiency at operating conditions: 28.2%

The reduction in turbine power from 100 kW_e is due to the operating conditions. Although the altitude is constrained by location, the turbine power and efficiency could be increased to 83 kW_e and 29.7% respectively by implementing inlet air cooling to 15 ℃. This is not considered at present. The solar collection system parameters are:

- Heliostat area: 13.4 m^2
- Annual heliostat field efficiency: 0.67%
- Design point Direct Normal Irradiance (DNI): 950 W/m^2
- High temperature receiver efficiency: 70 %
- Receiver and storage inlet pressure: 396 kPa_{abs}

Hourly DNI data, in the form of a Typical Meterological Year (TMY) is available from the International Weather for Energy Calculation (IWEC) database for Johannesburg. This city is located 50 km from the plant location and experiences similar weather patterns. The TMY allows for performance calculations based on statistically probable weather data. The excess energy available for storage is calculated using:

$$E_{\text{stored}} = \int_0^{t_c} \left(\text{DNI} \times N_{\text{hel}} A_{\text{hel}} \eta_{\text{hel}} \eta_{\text{rec}} - \dot{Q}_{\text{turb}} \right) \mathrm{d}t \tag{23}$$

Four SMs were investigated to determine a viable plant design (excluding cost analysis), able to incorporate the proposed thermal storage system. The DNI profile for each day in the TMY was analysed and the excess energy available for storage was calculated using Eq.(23). The thermal energy was then converted into a nominal hourly value using the turbine thermal power requirement $\dot{Q}_{\text{turb}}$. As shown in Fig. 6, six hours of thermal storage is not feasible with a solar multiple of 1.5 or 1.8. For a SM of 2.1, 31% of days in the TMY will supply six or more hours of thermal storage, while 52% of days will supply three or more hours of thermal storage. If the SM is increased to 2.4, 41% of

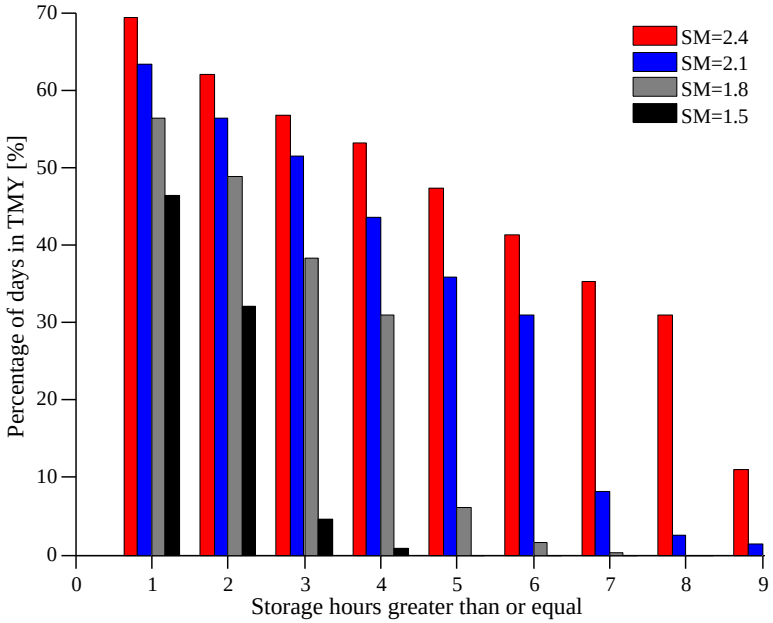

Figure 6: Number of days in TMY with storage greater than or equal to hourly values between 1 and 9 hours

days will supply six or more hours of thermal storage, and 57% of days will provide three or more hours of thermal storage.

From an energy yield perspective it is naturally beneficial to maximise the SM. However the overall capital cost of the plant is strongly dependent on the choice of SM. This is primarily related to the size of the required heliostat field. A detailed financial optimisation of the SM with respect to the Levelised Cost of Electricity (LCOE) is beyond the scope of this work. Therefore the chosen SM is based on energy considerations. Figure 6 indicates that for a SM of 2.4 a large number of days in the TMY are able to supply more than six hours of storage. However, once the TES is fully charged any further excess energy cannot be stored. Figure 7 presents the total energy stored throughout the TMY for six hours of storage, compared to the total energy available for storage. The results reveal that the level of wasted energy is significantly higher for the SM of 2.4 than the solar multiple of 2.1. Therefore a SM of 2.1 was chosen for this work.

For comparison Amsbeck et al. (2010) chose a solar multiple of 2.7 for a nine hour storage system for the T100 gas turbine at a plant location that receives an annual DNI of 2015 kWh/m^2/yr (Amsbeck et al., 2008). The total sum of the DNI profiles taken from the TMY for the current plant location amounts to 1782 kWh/m^2/yr. The use of an annual heliostat field efficiency in Eq.(23) is an approximation, as the actual heliostat efficiency will vary according to the relative position of the sun to the heliostat field. A more detailed plant model would take this into account. As the aim of this study is to investigate the storage component of the design thus this approximation is acceptable.

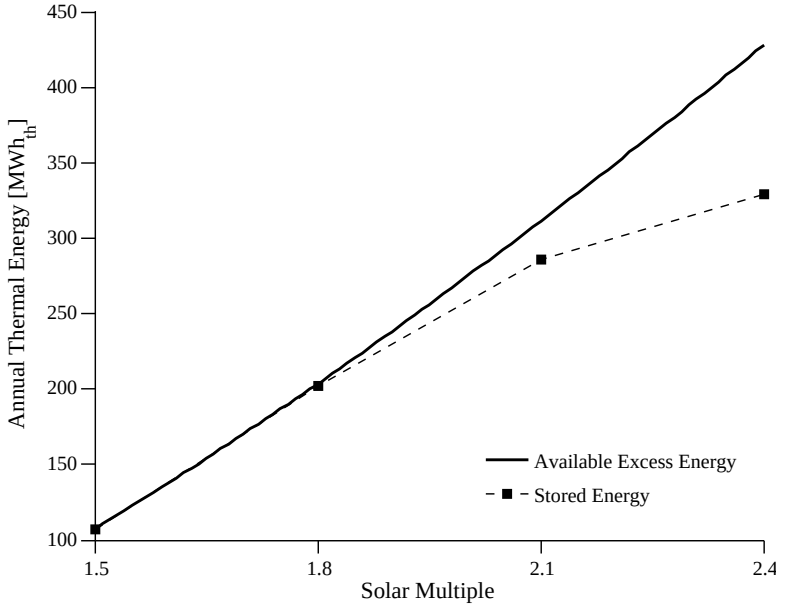

Figure 7: Analysis of the of annual energy available for storage as a function of SM, excluding partial discharging

7.2. Design day

Figure 8 shows the DNI profile taken from the TMY for typical clear summer and winter days. The summer day has a higher peak and wider spread. across the day. However, an analysis of the TMY showed that Pretoria experiences a

significantly higher number of clear days in winter than summer, due to cloud cover. Thus the clear winter day DNI profile was chosen for the design study. This day is able to fill the storage to maximum capacity.

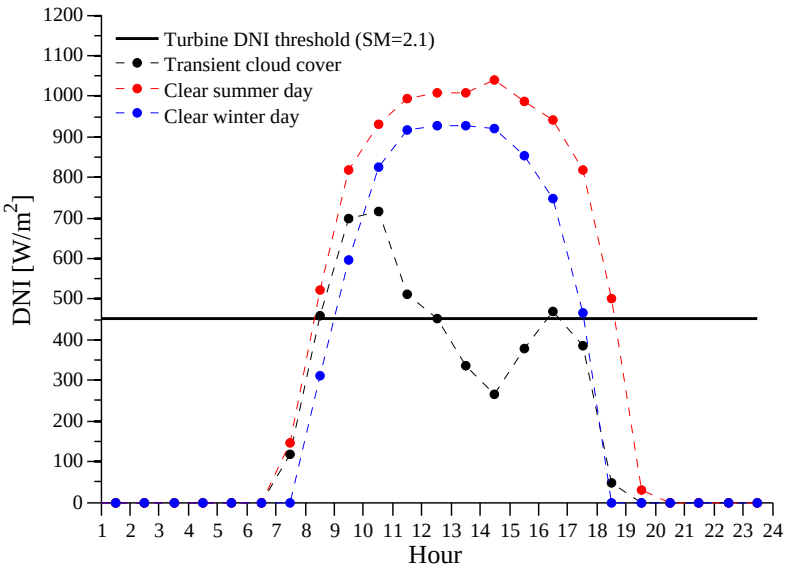

Figure 8: DNI profile for clear summer and winter days

7.3. Utilisation factor

Unlike latent heat TES, sensible heat TES is non-isothermal. Therefore these systems must be over-sized, in order to account for the storage material that does not undergo the full temperature change between the charge and discharge temperatures. The efficient use of the storage material is vital to cost reductions, as over-sizing of the system increases the storage mass and volume. This is particularly important in a pressurised environment where a premium is placed upon the storage volume. The concept of a utilisation factor is introduced to benchmark the amount of thermal energy that is recovered from each storage configuration, relative to the total theoretical maximum that can be stored:

$$F = \frac{\int_{t_c}^{t_d} \dot{m}_d c_f \left(T_d(t) - 873\right) \, \mathrm{d}t}{m_s c_s \Delta T_{\mathrm{rec}}} \tag{24}$$

where the discharge temperature is defined as:

$$T_d(t) = \frac{2\pi\rho_f}{\dot{m}_d} \int_0^R U_z(r) T_f(0,r) r \, \mathrm{d}r \tag{25}$$

There are three factors that affect the utilisation factor: 1) the maximum allowable temperature that the packed bed base ($z = L$) reaches during the charging cycle; 2) the maximum allowable decrease in discharging temperature; 3) heat losses through the storage wall.

In an ideal storage system the base of the packed bed would reach 950 ℃ during the charging cycle, thus maximising the amount of thermal energy stored. However, the hot air exiting the packed bed is in direct contact with the mesh support grid for the ceramic particles and the blower. In order to avoid the use of costly nickel based super-alloys, these components should not exceed 700 ℃ (Glück et al., 1991). Figure 9 shows the effect of the maximum base temperature on F, for a packed bed configuration of $\alpha = 3$ and $d_p = 10, 50$ mm. Raising the allowable base temperature from 650 ℃ to 750 ℃ increases F by a maximum of 6% and 15% for the 10 mm and 50 mm particles respectively. The effect is more pronounced for the larger particles due to the lower rate of convective heat transfer.

During the discharge cycle the exit temperature of the fluid (discharging temperature) starts to decrease over time as the thermocline approaches the bed exit. Once the discharging temperature decreases to below the specified limit the storage is considered to to depleted and the discharging cycle is stopped. The allowable decrease in discharge temperature is dependent on the choice of operating strategy for the SGT. If the system is designed to operate on solar energy only (no hybridisation), the discharge temperature should remain close to 950 ℃ and not decrease below 850 ℃. At 850 ℃ the turbine power is already significantly reduced (52 $\mathrm{kW_e}$ assuming 28.2% conversion efficiency). If hybridisation is included then the combustion chamber can be used to boost the turbine inlet temperature to 950 ℃. As shown in Fig. 9, the inclusion of hybridisation increases F for the TES, as a larger portion of energy can be extracted from the storage before it is considered depleted.

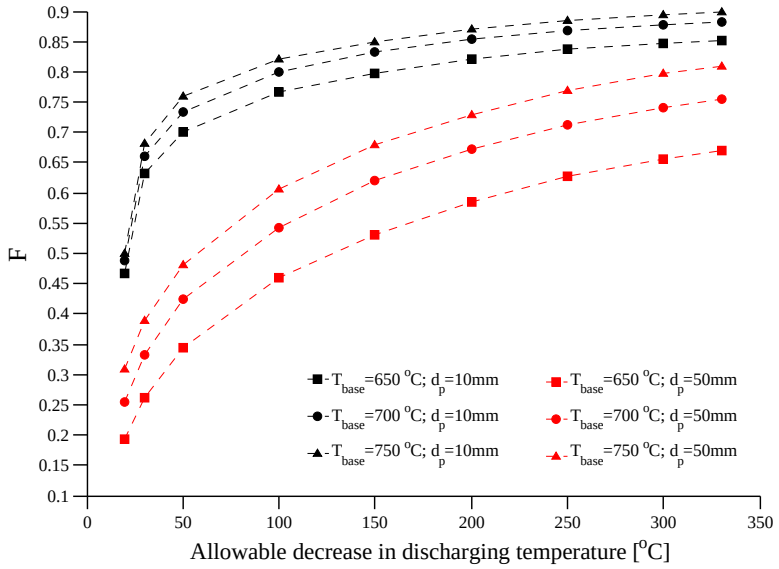

Figure 9: Utilisation factor as a function of maximum base temperature and allowable decrease in discharging temperature

7.4. Thermocline shape

The term thermocline refers to the shape of the axial temperature profile between the 'hot' (950 ℃) and 'cold' (600 ℃) zones in the packed bed. The gradient of the thermocline influences the utilisation factor. A steep thermocline gradient allows for a large portion of the packed bed mass to be heated to 950 ℃ before the base reaches the temperature limit. Figure 10 presents the shape of the thermocline for various packed bed configurations at the point when the charging cycle is complete. In the current research a conservative temperature limit of 650 ℃ was imposed on the base.

The gradient of the thermocline is dependent on the convective heat transfer between the fluid and solid particles. Decreasing the particle size increases the surface area for heat exchange, while increasing the aspect ratio increases the convective heat transfer coefficient. Improved convective heat transfer increases the storage efficiency and utilisation factor.

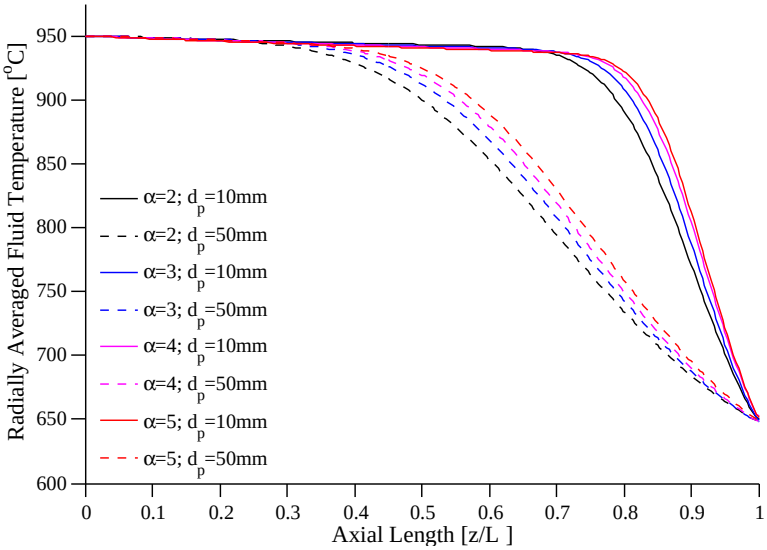

Figure 10: Charging thermocline shape when $T_{\text{base}} = 650$ ℃ (clear winter day)

7.5. Pressure drop and blower power requirement

The increase in convective heat transfer in the packed bed must be balanced against the increase in pressure drop, as the gas turbine performance is sensitive to this parameter. One of the benefits of the pressurised system is the density related decrease in the volumetric flow rate. Figure 11 shows the effect of aspect ratio and particle diameter on the pressure drop during the discharging phase. In discharging mode the pressure drop is shown to be below 4.5 kPa for all bed configurations that were simulated. Under worst case scenario of $\alpha = 5$ and $d_p = 10$ mm, the pressure drop is close to that of the benchmark receiver (4 kPa). Thus the pressure drop during discharging is acceptable for all configurations, under discharging conditions.

In charging mode the blower must circulate the air between the packed bed and the receiver. The electrical power requirement for the blower is calculated using:

$$\dot{E}_{\text{blower}} = \frac{1}{\eta_{\text{blower}}} \frac{\dot{m}_c}{\rho_f} \Big(\Delta P_{\text{bed}} + \Delta P_{\text{rec}} \Big) \tag{26}$$

The pressure drop across the packed bed was calculated using Eq.(5). Due to

the lack of a detailed receiver design an initial estimate of the receiver pressure drop was made based on measurements taken during testing of the SOLGATE receiver. As described by Spelling (2013), the receiver pressure drop can be estimated by scaling the conditions relative to the SOLGATE receiver. In future work, once detailed receiver designs are conducted the receiver pressure drop can be more accurately modelled. The pressure drop is estimated by:

$$\frac{\Delta P_{\mathrm{rec}}}{\Delta P_{\mathrm{refos}}} = \left(\frac{G_{\mathrm{rec}}}{G_{\mathrm{refos}}}\right)\left(\frac{P_{\mathrm{refos}}}{P_{\mathrm{rec}}}\right)\left(\frac{T_{\mathrm{rec}}}{T_{\mathrm{refos}}}\right) \tag{27}$$

where $\Delta P_{\mathrm{refos}} = 40$ mBar, $G_{\mathrm{refos}} = 1.063$ kg/sm^2, $P_{\mathrm{refos}} = 6.5$ bar, $T_{\mathrm{refos}} = 700$ ℃.

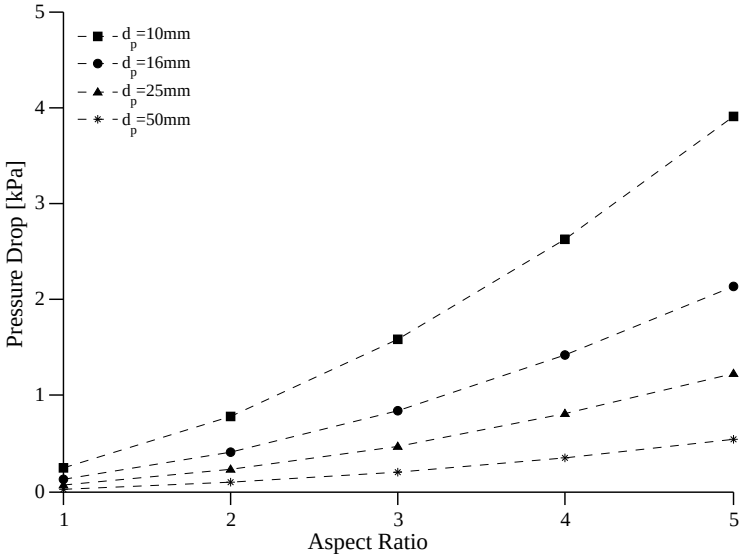

Figure 11: Pressure drop across the packed bed, calculated using Eq.(5) and $\dot{m}_f = 0.64$ kg/s

Figure 12 shows that most of the blower power is used to circulate the air through the receiver. For $\alpha = 5$ and $d_p = 10$ mm the blower power reaches 7.3 $\mathrm{kW_e}$, which is 10% of the electrical power produced by the turbine. The sudden decrease in power requirements, shown in Fig. 12, occurs when the storage charging is stopped as the base temperature has reached its limit. Even with very low pressure drop across the packed bed, the blower power requirements

reach 5 kW_e due to the receiver pressure drop. This could be overcome by including a second receiver to use for charging the storage. This would avoid the increased mass flow and associated pressure drop across the primary receiver.

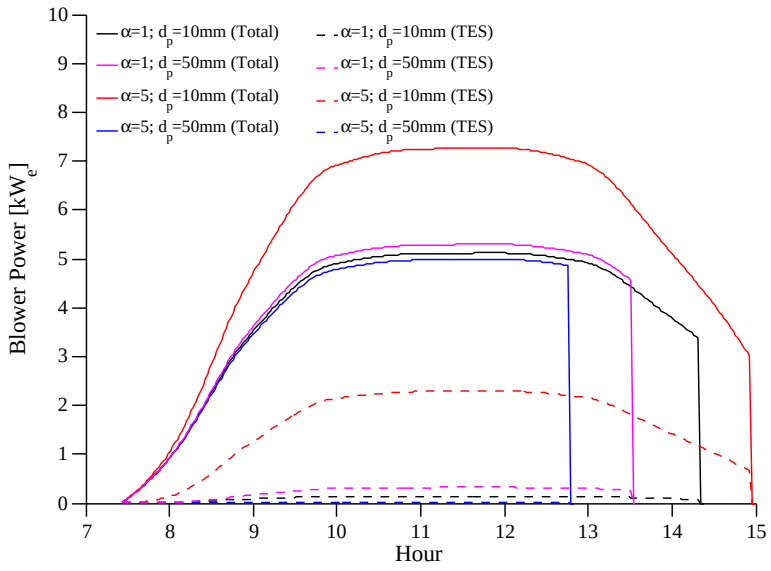

Figure 12: Blower power requirements during the charging cycle on a clear winters day

7.6. Storage efficiency

The efficiency of each storage configuration is calculated using Eq.(28). The numerator represents the total thermal energy extracted from the TES during discharging. The denominator represents the total thermal energy supplied to the packed bed as well as the energy supplied to operate the blower. The blower electrical energy is converted into thermal energy using the efficiency of the gas turbine ($\eta_{\text{turb}} = 0.282$ at specified conditions).

$$\xi = \frac{Q_{\text{th,extracted}}}{Q_{\text{th,supplied}} + Q_{\Delta P,\text{supplied}}} \tag{28}$$

where:

$$Q_{\text{th,extracted}} = \int_{t_c}^{t_d} \dot{m}_d c_f \Big(T_d(t) - 873 \Big) \, \mathrm{d}t \tag{29}$$

$$Q_{\text{th,supplied}} = \int_0^{t_c} \dot{m}_c c_f \Big(1223 - T_b(t)\Big)\,\mathrm{d}t \tag{30}$$

$$Q_{\Delta P,\text{supplied}} = \frac{1}{\eta_{\text{turb}}} \int_0^{t_c} \dot{E}_{\text{blower}}(t)\,\mathrm{d}t \tag{31}$$

8. Results

The parametric design study includes the operation of the storage with and without hybridisation. During the discharging cycle the storage is considered to be depleted when the discharge temperature drops below 620 ℃ for TES+hybridisation; and below 850 ℃ for TES only. The results for the storage efficiencies and utilisation factors are presented in Figs. 13 and 14 respectively. The advantages of combining TES with fossil fuel hybridisation are clear. The boosting of the discharge temperature allows for the more energy to be extracted from the storage before it is considered depleted, resulting in an increase in storage efficiency and utilisation factor. As shown in Fig. 13, the storage efficiency decreases with increasing aspect ratio for TES+hybridisation. This is caused by the increase in pressure drop and heat losses through the wall. The particle diameter does not have large influence on the efficiency for this case. The largest 50 mm particles have efficiencies between 0.4% and 1.4% lower than the 10 mm particle diameters for various aspect ratios. Increasing the aspect ratio from 1 to 5 decreases the efficiency by between 4.1% and 5%, depending on the particle diameter. For the case of TES only, the decrease in convective heat transfer at low aspect ratios, results in lower storage efficiencies. The choice of particle diameter has a more pronounced effect on storage efficiency for the TES only case. Using the 10 mm particles improves the efficiency, by up to 27%, when compared to the 50 mm particles.

Both test cases exhibit small improvements in utilisation factor with increasing aspect ratio. The choice of particle diameter plays a more important role. The 10 mm particles maximise the utilisation factor for both TES+hybridisation

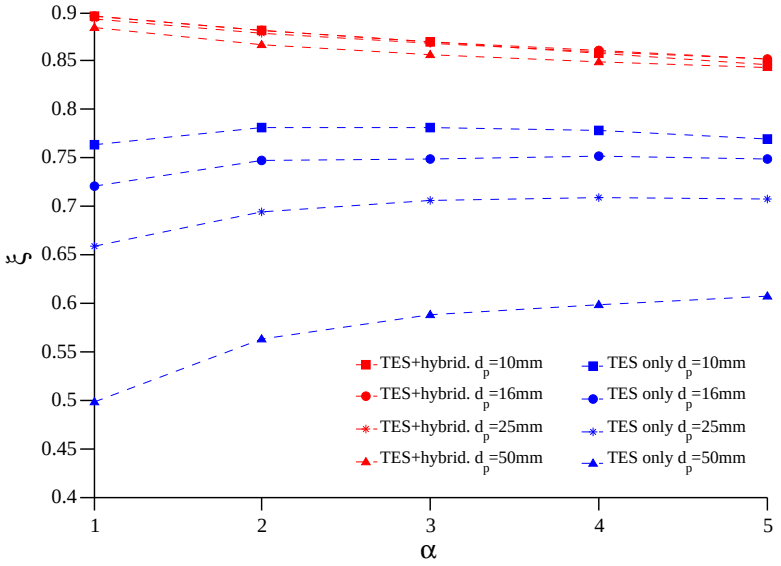

Figure 13: Storage efficiencies from design study

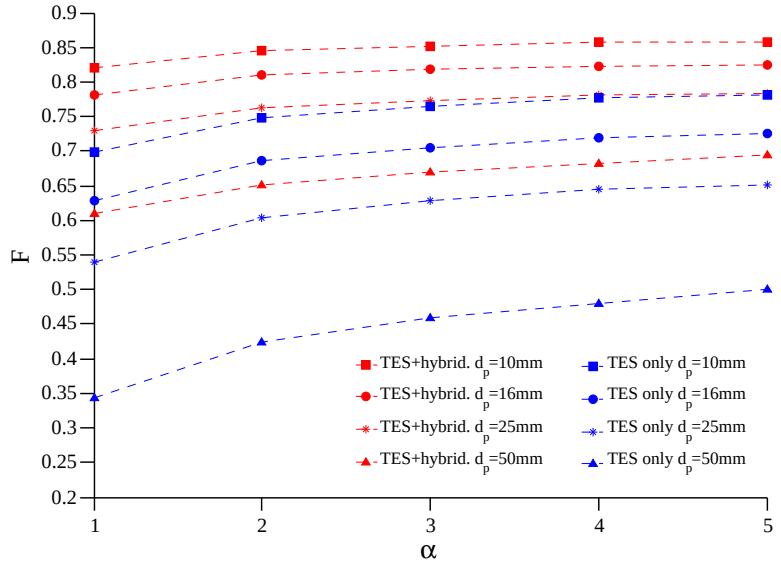

Figure 14: Utilisation factors from design study

and TES only cases. Table 2 provides insight into the energy stored and discharged by each storage configuration. In order to achieve a nominal six hours of storage, the TES system should be able to store a total of 1553 kWh_{th}. At a SM of 2.1 the design day that was chosen can supply a total of 1782 kWh_{th} of excess thermal energy. As shown in Table 2 only the storage configurations 1, 5, 6, 9, 10, 13, 14, 15, 17, 18, 19 can store more than 1553 kWh_{th} before the base temperature reaches its limit. In terms of energy extracted only configurations 5, 9, 13, 17 can supply more than 1553 kWh_{th} for the case of TES+hybridisation. These configurations also have the highest blower requirements of 6-7.3 kW_e. Configurations 10, 14, 18 can supply greater than 97% of the targeted energy value for TES+hybridisation. For the TES only case, configuration 17 is able to discharge 93% of the targeted energy value. A second design iteration can be performed with an increase in storage volume to achieve 100% of the specified discharge energy.

9. Conclusions

A high temperature thermal storage system was proposed in order to increase the solar share of a SGT for off the grid power generation. A detailed model of the system was developed and solved using a finite element approach. The model was successfully validated against experimental data from a purpose built test facility. Alumina was identified as an effective high temperature storage material due to its low cost and high volumetric energy storage density. The validated TES model was used to conduct a parametric design study to determine the optimal storage configuration for a 7 m^3 packed bed. The results showed that the inclusion of hybridisation is important in order to increase the storage efficiency and utilisation factor. For each analysed storage configuration the level of stored energy increased with increasing the aspect ratio and decreasing the particle diameter. For the case of TES+hybridisation the configuration of $\alpha = 2$ and $d_p = 10$ mm is preferable, yielding 1559 kWh_{th} of energy discharged at a storage efficiency of 88% and utilisation factor of 85%. If hybridisation is not allowed

for the preferable configuration is $\alpha = 4$ and $d_p = 10$ mm, yielding 1435 $\mathrm{kWh_{th}}$ energy discharged at a storage efficiency of 78% and utilisation factor of 78%.

Table 2: Results of parametric design study for nominal six hour TES

Config. Num.	α	d_p [mm]	Q_{supply} [kWh_{th}]	Q_{extract} [1] [kWh_{th}]	Q_{extract} [2] [kWh_{th}]	$E_{\text{blower}}/\eta_{\text{turb}}$ [kWh_{th}]
1	1	10	1588	1517 (0.98)	1291 (0.83)	104
2		16	1510	1442 (0.93)	1159 (0.75)	98
3		25	1411	1343 (0.86)	991 (0.64)	92
4		50	1182	1113 (0.71)	626 (0.40)	77
5	2	10	1656	1559 (1.00)	1381 (0.89)	114
6		16	1588	1492 (0.96)	1265 (0.81)	106
7		25	1495	1399 (0.9)	1106 (0.71)	99
8		50	1282	1184 (0.76)	769 (0.50)	84
9	3	10	1684	1572 (1.01)	1412 (0.91)	124
10		16	1620	1507 (0.97)	1298 (0.84)	112
11		25	1530	1417 (0.91)	1152 (0.74)	103
12		50	1329	1214 (0.78)	832 (0.54)	88
13	4	10	1705	1581 (1.02)	1435 (0.92)	137
14		16	1638	1513 (0.97)	1320 (0.85)	120
15		25	1556	1430 (0.92)	1179 (0.76)	108
16		50	1360	1232 (0.79)	868 (0.56)	92
17	5	10	1716	1582 (1.02)	1439 (0.93)	153
18		16	1651	1516 (0.98)	1331 (0.86)	128
19		25	1570	1434 (0.92)	1191 (0.77)	114
20		50	1389	1251 (0.81)	902 (0.58)	95

[1] TES+hybridisation case

[2] TES only case

bracketed values indicate fraction of energy discharged relative to 1553 kWh_{th}

10. Acknowledgements

The authors would like to thank the Council for Scientific and Industrial Research (CSIR) for funding to perform this research, and the South African National Energy Development Institute (SANEDI) for equipment funding.

Nomenclature

A	area ..... m^2	h_p	inter-phase heat transfer coefficient ..... $\mathrm{W/m^2K}$
a_p	particle surface area to volume ratio ..... $\mathrm{m^{-1}}$	k	thermal conductivity .. W/mK
c	specific heat capacity at constant pressure ..... J/kgK	k_{eff}	effective thermal conductivity W/mK
C_A	inertial Ergun coefficient	L_z	packed bed length ..... m
C_B	viscous Ergun coefficient	m	mass ..... kg
C_d	dispersion coefficient	$\dot{m}$	mass flow rate ..... kg/s
d_p	particle diameter ..... m	N	number .....
DNI	direct normal irradiance W/m^2	P	pressure ..... Pa
$\dot{E}$	electrical power ..... J/s	ΔP	pressure drop ..... Pa
f_1	Brinkman equation viscous coefficient ..... $\mathrm{kg/m^2s}$	Q	thermal energy ..... J
f_2	Brinkman equation inertial coefficient ..... $\mathrm{kgs^2/m^3}$	Q_{vol}	volumetric energy storage density ..... $\mathrm{J/m^3}$
F	utilisation factor	$\dot{Q}$	thermal power ..... J/s
G	mass flux ..... $\mathrm{kg/sm^2}$	q	heat flux ..... $\mathrm{W/m^2}$
H	Hermite polynomials	R	packed bed radius ..... m
h_{fs}	modified heat transfer coefficient ..... $\mathrm{W/m^2K}$	r	radial coordinate ..... m
		T	temperature ..... K
		t	time ..... s

u	local element radial coordinate
U_z	axial superficial fluid velocity m/s
v	local element axial coordinate
z	axial coordinate ..... m

Greek Symbols

α	packed bed aspect ratio (L_z/D) .....
ϵ	void fraction .....
ϵ_∞	bed centre void fraction .....
η	efficiency .....
μ	dynamic viscosity ..... Pa s
μ_{eff}	effective fluid viscosity ... Pa s
ϕ	unknown spline coefficients ...
ρ	density ..... kg/m^3
ξ	storage efficiency .....

Superscripts

ab	finite element location
n	time step .....

Subscripts

a	radial element boundary
b	axial element boundary
bed	solar receiver .....
c	charging .....
d	discharging .....
f	fluid phase .....
hel	heliostat .....
rec	solar receiver .....
ref	REFOS receiver .....
s	solid phase .....
turb	gas turbine .....
w	wall .....

Non-Dimensional Variables

$\text{Bi}_p = \frac{h_{\text{fs}} d_p}{2k_s}$	Particle Biot number ....
$\text{Nu}_p = \frac{h_{\text{fs}} d_p}{k_f}$	Particle Nusselt number.
$\text{Pr} = \frac{c_f \mu_f}{k_f}$	Prandtl number .....
$\text{Re}_p = \frac{\rho_f U_z d_p}{\mu_f}$	Particle Reynolds number .....

References

Adebiyi, G. A., Nsofor, E. C., Steele, W. G., Jalalzadeh-Azar, A. A., 1998. Parametric study on the operating efficiencies of a packed bed for high-temperature sensible heat storage. ASME Journal of Solar Energy Engineering 120 (1), 2–13.

Amsbeck, L., Buck, R., Heller, P., Jedamski, J., Uhlig, R., 2008. Development

of a tube receiver for a solar-hybrid microturbine system. In: Proceedings of 14th SolarPACES Conference, Las Vegas. pp. 4–7.

Amsbeck, L., Denk, T., Ebert, M., Gertig, C., Heller, P., Herrmann, P., ... & Uhlig, R., 2010. Test of a solar-hybrid microturbine system and evaluation of storage deployment. In: 16th SolarPACES symposium, Perpignan, France.

Aora, n.d. Http://aora-solar.com/active-sites, Acessed 31/10/2014.

Avila-Marin, A. L., Alvarez-Lara, M., Fernandez-Reche, J., 2014. A regenerative heat storage system for central receiver technology working with atmospheric air. Energy Procedia 49, 705–714.

Beasley, D. E., Clark, J. A., 1984. Transient response of a packed bed for thermal energy storage. International Journal of Heat and Mass Transfer 27 (9), 1659–1669.

Bindra, H., Bueno, P., Morris, J. F., Shinnar, R., 2013. Thermal analysis and exergy evaluation of packed bed thermal storage systems. Applied Thermal Engineering 52 (2), 255–263.

Bradshaw, A. V., Johnson, A., McLachlan, N. H., Chiu, Y. T., 1970. Heat transfer between air and nitrogen and packed beds of non-reacting solids. Transactions of the Institute of Chemical Engineers 48, T77–T84.

Bradshaw, R. W., Siegel, N. P., 2008. Molten nitrate salt development for thermal energy storage in parabolic trough solar power systems. In: ASME 2008 2nd International Conference on Energy Sustainability collocated with the Heat Transfer, Fluids Engineering, and 3rd Energy Nanotechnology Conferences. American Society of Mechanical Engineers, pp. 631–637.

Du Toit, C. G., Rousseau, P. G., Greyvenstein, G. P., Landman, W. A., 2006. A systems CFD model of a packed bed high temperature gas cooled nuclear reactor. International Journal of Thermal Sciences 45 (10), 70–85.

Finlayson, B. A., 1980. Orthogonal collocation on finite elements - progress and potential. Mathematics and Computers in Simulation 22 (1), 11–17.

Giese, M., Rottschäfer, K., Vortmeyer, D., 1998. Measured and modeled superficial flow profiles in packed beds with liquid flow. American Institute of Chemical Engineers Journal 44 (2), 484–490.

Glück, A., Tamme, R., Kalfa, H., Streuber, C., 1991. Investigation of high temperature storage materials in a technical scale test facility. Solar Energy Materials 24 (1), 240–248.

Gunn, D. J., 1978. Transfer of heat or mass to particles in fixed and fluidised beds. International Journal of Heat and Mass Transfer 21 (4), 467–476.

Hunt, M. L., Tien, C. L., 1990. Non-Darcian flow, heat and mass transfer in catalytic packed-bed reactors. Chemical Engineering Science 45 (1), 55–63.

IAEA, 2001. Heat transport and afterheat removal for gas-cooled reactors under accident conditions-technical report IAEA-TECDOC-1163.

Ismail, K. A., Stuginsky, R., 1999. A parametric study on possible fixed bed models for pcm and sensible heat storage. Applied Thermal Engineering 19 (7), 757–788.

Jalalzadeh-Azar, A. A., Steele, W. G., Adebiyi, G. A., 1996. Heat transfer in a high-temperature packed bed thermal energy storage system - roles of radiation and intraparticle conduction. Journal of Energy Resources Technology 118 (1), 50–57.

Jalalzadeh-Azar, A. A., Steele, W. G., Adebiyi, G. A., 1997. Performance comparison of high-temperature packed bed operation with PCM and sensible heat pellets. International Journal of Energy Research 21 (11), 1039–1052.

Jeffreson, C. P., 1972. Prediction of breakthrough curves in packed beds: 1. applicability of single parameter models. American Institute of Chemical Engineers Journal 18 (2), 409–416.

Klein, P., Roos, T., Sheer, T. J., 2014a. High temperature thermal storage for solar gas turbines using encapsulated phase change materials. In: The 2nd Southern African Solar Energy Conference (SASEC).

Klein, P., Roos, T., Sheer, T. J., 2014b. Experimental investigation into a packed bed thermal storage solution for solar gas turbine systems. Energy Procedia, 49, 840-849. 49, 840–849.

Klinkenberg, A., 1948. Numerical evaluation of equations describing transient heat and mass transfer in packed solids. Industrial & Engineering Chemistry 40 (10), 1992–1994.

Macdonald, I. F., El-Sayed, M. S., Mow, K., Dullien, F. A., 1979. Flow through porous media-the ergun equation revisited. Industrial & Engineering Chemistry Fundamentals 18 (3), 199–208.

Modi, A., Pérez-Segarra, C. D., 2014. Thermocline thermal storage systems for concentrated solar power plants: One-dimensional numerical model and comparative analysis. Solar Energy 100, 84–93.

Mongibello, L., Atrigna, M., Graditi, G., 2013. Parametric analysis of a high temperature sensible heat storage system by numerical simulations. Journal of Solar Energy Engineering 135 (4), 041010.

Niessen, H. F., Stöcker, B., 1997. Data sets of the sana experiment 1994-1996. Tech. rep., JUEL-3409. Forschungszentrum Jülich GmbH.

Pacheco, J. E., Showalter, S. K .and Kolb, W. J., 2002. Development of a molten-salt thermocline thermal storage system for parabolic trough plants. Journal of Solar Energy Engineering 124 (2), 153–159.

Roos, T. H., Rubin, N., Maliage, M., Klein, P., Dunn, D., Perumal, S., 2015. DPSS IRIP Progress Report for 2010/2011 and 2011/2012. CSIR Project Report, DPSS ASC2011/046.

Schumann, T. E., 1929. Heat transfer: a liquid flowing through a porous prism. Journal Franklin Institute 208 (3), 405–416.

Spelling, J., 2013. Hybrid solar gas-turbine power plants: A thermoeconomic analysis. Ph.D. thesis, KTH University.

Tamme, R., Grozinger, U., Gluck, A., Kanwischer, H., Neitzel, U., 1990. Advanced regenerator media for industrial and solar thermal applications. In: Energy Conversion Engineering Conference. Vol. 4. pp. 218–221.

Too, S., Olivares, R., Benito, R., Kim, J. S., Duffy, G., Edwards, J., 2012. High temperature thermal energy storage systems for open-cycle solar air brayton plant.

Turbec, 2006. Technical documentation Microturbine Turbec T100.

Visser, C. J., Malan, A. G., Meyer, J. P., 2008. An artificial compressibility algorithm for modelling natural convection in saturated packed pebble beds: a heterogeneous approach. International Journal for Numerical Methods in Engineering 75 (10), 1214–1237.

Vortmeyer, D., Schuster, J., 1983. Evaluation of steady flow profiles in rectangular and circular packed beds by a variational method. Chemical Engineering Science 38 (10), 1691–1699.

Wakao, N., Kaguei, S., 1982. Heat and mass transfer in packed beds. Vol. 1. Taylor & Francis.

Xu, C., Wang, Z., He, Y., Li, X., Bai, F., 2012a. Sensitivity analysis of the numerical study on the thermal performance of a packed-bed molten salt thermocline thermal storage system. Applied Energy 92, 65–75.

Xu, C., Wang, Z., He, Y., Li, X., Bai, F., 2012b. Parametric study and standby behavior of a packed-bed molten salt thermocline thermal storage system. Renewable Energy 48, 1–9.

Yang, Z., Garimella, S. V., 2010a. Thermal analysis of solar thermal energy storage in a molten-salt thermocline. Solar energy 84 (6), 974–985.

Yang, Z., Garimella, S. V., 2010b. Molten-salt thermal energy storage in thermoclines under different environmental boundary conditions. Applied Energy 87 (11), 3322–3329.

Zanganeh, G., Pedretti, A., Zavattoni, S., Barbato, M., Steinfeld, A., 2012. Packed-bed thermal storage for concentrated solar power-pilot-scale demonstration and industrial-scale design. Solar Energy 86 (10), 3084–3098.

Zunft, S., Hänel, M., Krüger, M., Dreißigacker, V., 2014. A design study for regenerator-type heat storage in solar tower plants–results and conclusions of the hotspot project. Energy Procedia 49, 1088–1096.